The Astrophysical Journal, 698:580–593, 2009 June 10 doi:10.1088/0004-637X/698/1/580

GALAXY CLUSTERS: A NOVEL LOOK AT DIFFUSE BARYONS WITHSTANDING DARK MATTER GRAVITY

A. Cavaliere[1,2], A. Lapi[1,3], and R. Fusco-Femiano[4]
[1] Dip. Fisica, Univ. "Tor Vergata," Via Ricerca Scientifica 1, 00133 Roma, Italy
[2] Accademia Nazionale dei Lincei, Via Lungara 10, 00165 Roma, Italy
[3] Astrophysics Sector, SISSA/ISAS, Via Beirut 2-4, 34014 Trieste, Italy
[4] INAF−Istituto di Astrofisica Spaziale e Fisica Cosmica, Via Fosso del Cavaliere, 00133 Roma, Italy
Received 2008 October 23; accepted 2009 March 31; published 2009 May 21

ABSTRACT

In galaxy clusters, the equilibria of the intracluster plasma (ICP) and of the gravitationally dominant dark matter (DM) are governed by the hydrostatic equation and by the Jeans equation, respectively; in either case gravity is withstood by the corresponding, entropy-modulated pressure. Jeans, with the DM "entropy" set to $K \propto r^{\alpha}$ and $\alpha \approx 1.25$–1.3 applying from groups to rich clusters, yields our radial *α-profiles*; these, compared to the empirical Navarro–Frenk–White distribution, are flatter at the center and steeper in the outskirts as required by recent gravitational lensing data. In the ICP, on the other hand, the entropy run $k(r)$ is mainly shaped by shocks, as steadily set by supersonic accretion of gas at the cluster boundary, and intermittently driven from the center by merging events or by active galactic nuclei (AGNs); the resulting equilibrium is described by the exact yet simple formalism constituting our ICP *Supermodel*. With two parameters, this accurately represents the runs of density $n(r)$ and temperature $T(r)$ as required by up-to-date X-ray data on surface brightness and spectroscopy for both cool core (CC) and non-cool core (NCC) clusters; the former are marked by a middle temperature peak, whose location is predicted from rich clusters to groups. The Supermodel inversely links the inner runs of $n(r)$ and $T(r)$, and highlights their central scaling with entropy $n_c \propto k_c^{-1}$ and $T_c \propto k_c^{0.35}$, to yield radiative cooling times $t_c \approx 0.3\,(k_c/15\,\mathrm{keV\,cm^2})^{1.2}$ Gyr. We discuss the stability of the central values so focused: against radiative erosion of k_c in the cool dense conditions of CC clusters, that triggers recurrent AGN activities resetting it back; or against energy inputs from AGNs and mergers whose effects are saturated by the hot central conditions of NCC clusters. From the Supermodel, we also derive as limiting cases the classic polytropic β-models, and the "mirror" model with $T(r) \propto \sigma^2(r)$ suitable for NCC and CC clusters, respectively; these limiting cases highlight how the ICP temperature $T(r)$ strives to mirror the DM velocity dispersion $\sigma^2(r)$ away from energy and entropy injections. Finally, we discuss how the Supermodel connects information derived from X-ray and gravitational lensing observations.

Key words: dark matter – galaxies: clusters: general – gravitational lensing – methods: analytical – X-rays: galaxies: clusters

Online-only material: color figures

1. INTRODUCTION

Diffuse baryons and dark matter (DM) constitute the major components of clusters and groups of galaxies, with the former energized and shining by continual struggle against the latter.

The DM accounts for some 6/7 of the total masses $M \sim 10^{13}$–$10^{15}\,M_{\odot}$ from poor groups to rich clusters, making for average densities $\rho \sim 10^{-26}$ g cm^{-3} with its constituent ("collisionless") particles entertaining little or no interactions other than gravity. Thus, the DM sets the overall gravitational wells virialized within radii R up to a few Mpc, where all bodies in dynamical equilibrium—from single particles to whole galaxies—possess or acquire a one-dimensional velocity dispersion $\sigma^2 \approx GM/5R \sim 10^3$ km s^{-1}.

The bulk of the baryons, to a fraction again also close to 6/7, is found in the diffuse form of a hot intracluster *plasma* (the ICP), mostly comprised of protons with the neutralizing electrons at number densities $n \sim 10^{-3}$ cm^{-3}, and equilibrium temperatures $k_{\rm B}T \approx m_p\,\sigma^2/2 \sim 5$ keV ($k_{\rm B}$ being the Boltzmann constant and m_p the proton mass) well above most ionization potentials. This we know since Cavaliere et al. (1971) found in the first *Uhuru* data clear evidence of a new class of bright X-ray extragalactic sources associated with the deep, stable gravitational wells of the galaxy systems, emitting from the ICP they contain thermal bremsstrahlung powers $L_X \sim 2 \times 10^{-27}\,n^2\,R^3\,T^{1/2} \sim 10^{42}$–$10^{45}$ erg s^{-1}. The notion has been nailed down beyond all doubts by observations of the extended nature of these sources (Gursky et al. 1972) and of high excitation, coronal-like lines (Mitchell et al. 1976; Serlemitsos et al. 1977; see also Sarazin 1988) that also pointed toward definite, somewhat subsolar metallicities.

Such temperatures and densities make the ICP an extremely *good* plasma, in fact the best in the universe, as its constituent particles in the DM gravitational wells acquire a large kinetic relative to electrostatic energy (at mean separations $\bar{d} = n^{-1/3} \sim 10$ cm), their ratio being of order $k_{\rm B}BT/e^2\,n^{1/3} \sim 10^{12}$; this astounding value is to be compared with its counterparts: 10^3 in stellar interiors, or 3×10^5 in the prerecombination universe. This holds despite gravity being so exceedingly feeble at microscopic levels as to attain a mere $Gm_p^2/e^2 \sim 8 \times 10^{-37}$ of the strength that marks the electromagnetic interactions; it holds because the plasma condition

$$10^{12} \sim k_{\rm B}T/e^2n^{1/3} \equiv Gm_p^2/e^2 \times \bar{d}/10\,R \times \mathcal{N} \qquad (1)$$

is dominated by the huge number $\mathcal{N} \equiv M/m_p \sim 10^{73}$ expressing in proton units the total DM mass with its overwhelming gravity. As a result, the ICP at microscopic scales constitutes a very *simple*, nearly perfect gas of particles with 3 degrees of freedom and effective mass μm_p with $\mu \approx 0.6$. At intermediate scales of some 10 kpc, these sense mostly the electromagnetic

interactions; by the latter the electrons absorb or emit radiation, while the protons share their energy over a mean free path $\lambda_{pp} \approx 10\,(k_B T/5\,\mathrm{keV})^2\,(n/10^{-3}\,\mathrm{cm}^{-3})^{-1}$ kpc, with electrons following suit over some $40\lambda_{pp}$ toward full thermal equilibrium.

By the same token, the macrophysics at cluster scales gets interestingly *complex*, as the ICP constitutes a faithful *archive* preserving memory of the different energy inputs occurring throughout sizes of Mpc and over timescales of 10 Gyr. We shall see that the ICP physics is governed, in a nutshell, by the interplay of electromagnetic interactions transferring energy to the plasma, and of the DM bulk gravity proceeding to blend and readjust it over cluster scales.

To disentangle these processes, it will prove technically convenient to use two synthetic and formally analogous quantities. As for the ICP, the adiabat $k \equiv k_B T/n^{2/3}$ is straightforwardly related to the thermodynamic specific entropy $s = 3\,k_B/2 \times \log k +$ const. Usually named "entropy" for short, this quantity is endowed with time-honored, effective properties like: increasing (decreasing) by energy gains (losses) other than adiabatic compressions (expansions) and controlling the ICP settlement into gravitational wells.

As to the DM, the analogous quantity $K = \sigma^2/\rho^{2/3}$ is increasingly found to play—in spite of all the traditional objections leveled to defining "entropy" in a collisionless medium dominated by long range self-gravity like the DM—similar roles to a true entropy; in fact, it increases during the fast collapse with associated major mergers that set up the halo bulk, and stays put during the subsequent slow mass accretion producing a quiet development of the outskirts from the inside out. These two stages have been recently recognized in sophisticated *N*-body simulations that follow the development of halos embedding galaxies or galaxy systems from initial cold DM perturbations (e.g., Zhao et al. 2003; Diemand et al. 2007). From simulations, during quiet stages the simple power-law run $K(r) \propto r^\alpha$ is found to apply remarkably well with definite slopes close to $\alpha \approx 1.25$ throughout the structure's main body, as first stressed by Taylor & Navarro (2001) and confirmed by many others (e.g., Dehnen & McLaughlin 2005; Hoffman et al. 2007; Ascasibar & Gottlöber 2008; Vass et al. 2009; Navarro et al. 2009).

We shall find these two entropies to be most useful in computing and relating the macroscopic, static equilibria of DM and baryons in the *same* gravitational wells as set by the former. This is perceived on just inspecting their related equilibrium conditions for the density runs $n(r)$ and $\rho(r)$, namely, the hydrostatic versus the Jeans equation in the form

$$\frac{1}{\mu m_p\, n}\,\frac{d}{dr}(n^{5/3}\,k) = -\frac{GM(<r)}{r^2} = \frac{1}{\rho}\,\frac{d}{dr}(\rho^{5/3}\,K). \qquad (2)$$

While the rich contents of the second equality have been discussed in detail by Lapi & Cavaliere (2009a (hereafter LC09), see also Section 2 for a recap), in the present paper we will focus on the first equation. To this purpose, we make use of a physical model for $k(r)$ to derive the detailed pressure structure of the ICP.

Our approach develops the line extensively pursued in the literature at increasingly sophisticated levels. A simple isothermal or polytropic state has been adopted by, e.g., Cavaliere & Fusco-Femiano (1976, 1978), Balogh et al. (1999), Dos Santos & Doré (2002), and Ostriker et al. (2005). Refined models were based on a more articulated entropy run, consisting of an outer ramp produced by *gravitational* accretion shocks going on in the aftermath of cluster formation (see Tozzi & Norman 2001; Voit et al. 2003; Lapi et al. 2005, hereafter LCM05), plus a central entropy floor of *nongravitational* origin (e.g., Babul et al. 2002; Voit et al. 2002; Voit 2005). The latter may be contributed by a number of processes: cooling that selectively removes some low-entropy gas from the inner regions (see Bryan 2000; Voit & Bryan 2001; McCarthy et al. 2004); preheating of the ICP due to supernovae (SNe)/active galactic nuclei (AGNs) within the cluster progenitors (see LCM05; McCarthy et al. 2008); and the direct action within the cluster of central AGNs (Valageas & Silk 1999; Wu et al. 2000; Scannapieco & Oh 2004; LCM05). Additional gravitational events in the form of major mergers (Balogh et al. 2007; McCarthy et al. 2007) that now and then punctuate the equilibrium state of formed clusters (Cavaliere et al. 1999) may reach down to the center and enhance the entropy there.

Here, we improve over these previous studies in the following respects. As to the DM potential well, we adopt the physical α-profiles obtained from solving the Jeans equation rather than assuming the empirical Navarro–Frenk–White (NFW) fit (see Section 2). As to the ICP equilibrium, we present a novel analytical solution for the ICP density and temperature runs in terms of the ICP entropy distribution (see Section 3). The distribution that we use comprises an outer ramp and a central floor, marked by two parameters physically assessed in terms of steady, self-similar accretion shocks plus additional energy inputs due to central AGNs and mergers (see Section 3.1). We insert this entropy distribution in our equilibrium solution to obtain the ICP "Supermodel," that effectively represents with two ICP parameters the extended profiles of the X-ray surface brightness and temperature for either class: the cool core (CC) and the non-cool core (NCC) clusters, see Section 4. We discuss the stability against cooling and feedback of the ensuing central conditions (see Section 5). We also recover classic models for the ICP distribution of density and temperature as limiting cases of the Supermodel valid in different radial ranges and for different central entropy levels (see Section 6). We provide specific predictions for future X-ray observations of the ICP and model-independent tests of the entropy runs underlying the ICP Supermodel (see Section 7).

Throughout this work we adopt a standard, flat cosmology (see Spergel et al. 2007) with normalized matter density $\Omega_M = 0.27$, dark energy density $\Omega_\Lambda = 0.73$, and Hubble constant $H_0 = 72$ km s^{-1} Mpc^{-1}.

2. α-PROFILES FOR THE DM HALOS

From LC09, we recall for use in the present paper a number of basic features in the equilibrium of the DM halos embedding the ICP, as described by the Jeans equation with entropy $K \propto r^\alpha$ (see Section 1); in compact form this reads

$$\gamma = \frac{3}{5}\,\alpha + \frac{3}{5}\,\frac{v_c^2}{\sigma^2}. \qquad (3)$$

With $\alpha \equiv d\log K/d\log r$ set to a constant, this yields the changing density slope $\gamma(r) \equiv -d\log\rho/d\log r$ in terms of the increasing ratio to $\sigma^2(r)$ of the halo circular velocity squared $v_c^2(r) = GM(<r)/r$ that provides normalization and running estimates for the gravitational potential. The above equation provides the detailed cluster gravitational well, within which the ICP is to adjust.

The *physically* relevant values of α are pinned down from the structures' cosmogonic development. Based on the straightforward scaling laws $\sigma^2 \propto M/r$ and $r \propto M/\dot{M}^{2/3}$, it is seen that the entropy is to scale as $K \propto r\,M^{1/3}$, a run clearly implying a radial slope $\alpha \gtrsim 1$. The detailed time dependence of

the accretion rate $\dot{M}/M$ and the related quantities may be derived semianalytically within the standard ΛCDM cosmogony; the result for the allowed range is $\alpha = 1.25$–1.3 from groups to massive clusters, narrowed down to

$$\alpha \approx 1.27-1.3 \tag{4}$$

for average masses $M \sim 10^{14}$–$10^{15}\,M_\odot$ from poor to rich clusters of main interest here. In the structure's development, these values obtain at the transition epoch from the stage of fast collapse to that of slow accretion (relative to the running Hubble time), when the potential well attains its maximal depth marked by $\dot{M}\,t/M \sim 1$. Such a two-stage development turns out to be in tune with the intensive, detailed *N*-body simulations recalled in Section 1. In addition, the simulations support a value of α in the range above, which stays put from the center throughout the halo bulk as the late quasi-equilibrium configuration develops from the inside out.

These values may be inserted into the Jeans equation, to find (as pioneered by Taylor & Navarro 2001; Dehnen & McLaughlin 2005) all the *viable* solutions for $\rho(r)$, that we name "α-profiles" and illustrate in Figure 1. These feature a monotonic radial run satisfying physical central and outer boundary conditions, i.e., zero gravitational force (corresponding to a round minimum of the potential) and finite (hence definite) overall mass, respectively.

The ensuing behavior of the α-profiles, basic to the ICP equilibrium, is illustrated in the top panel of Figure 1, and highlighted by the analytic expressions of the slopes

$$\gamma_a = \tfrac{3}{5}\,\alpha, \quad \gamma_0 = 6 - 3\alpha, \quad \gamma_b = \tfrac{3}{2}\,(1+\alpha). \tag{5}$$

These start from the central ($r \to 0$) value $\gamma_a \approx 0.76$–0.78, progressively steepen to $\gamma_0 \approx 2.19$–2.1 at the point r_0 that marks the halo main body, and steepen further into the outskirts to the value $\gamma_b \approx 3.41$–3.44 at around the virial radius R before going into a final cutoff. The α-profiles are seen (see LC09) to correspond to a maximal value $\kappa_{\rm crit}(\alpha) = v_c^2/\sigma^2 \approx 2.6$–$2.5$ for the relative gravitational pull at the point $r = r_p \gtrsim r_0$, where $v_c^2(r)$ peaks (see also bottom panel of Figure 1). After Equation (3), this also implies at r_p a maximal slope $\gamma_p = 3\,(\alpha + k_{\rm crit})/5 \approx 2.32$–$2.28$.

At variance with the empirical NFW formula (Navarro et al. 1997) that features angled central potential and diverging mass, for the α-profiles the inner slope is considerably *flatter*, and the outer one is *steeper* as to result in a definite overall mass. The radial range $r > r_{-2}$ where the density profile is steeper than a reference slope $\gamma = 2$ may be specified in terms of the usual concentration parameter $c \equiv R/r_{-2}$ that may be viewed as a measure of central condensation and/or outskirts' extension. In up-to-date numerical simulations (see Zhao et al. 2003; Diemand et al. 2007), this is found to take on value $c \approx 3.5$ at the transition redshift z_t, and to increase thereafter to current values $c \approx 3.5\,(1+z_t)$ up to $c \approx 10$ for the fraction about 10% of rich clusters with early transition epoch $z_t \sim 1.5$. Instead, values $c \approx 4$–5 apply to the much more numerous clusters with recent transition epochs.

Another basic feature of the α-profiles is provided by the *peaked* run of the gravitationally acquired dispersion

$$\sigma^2(r) \propto K(r)\,\rho^{2/3}(r), \tag{6}$$

see bottom panel of Figure 1. Towering above the central and the outer drops related to the cold nature of the DM, the peak results

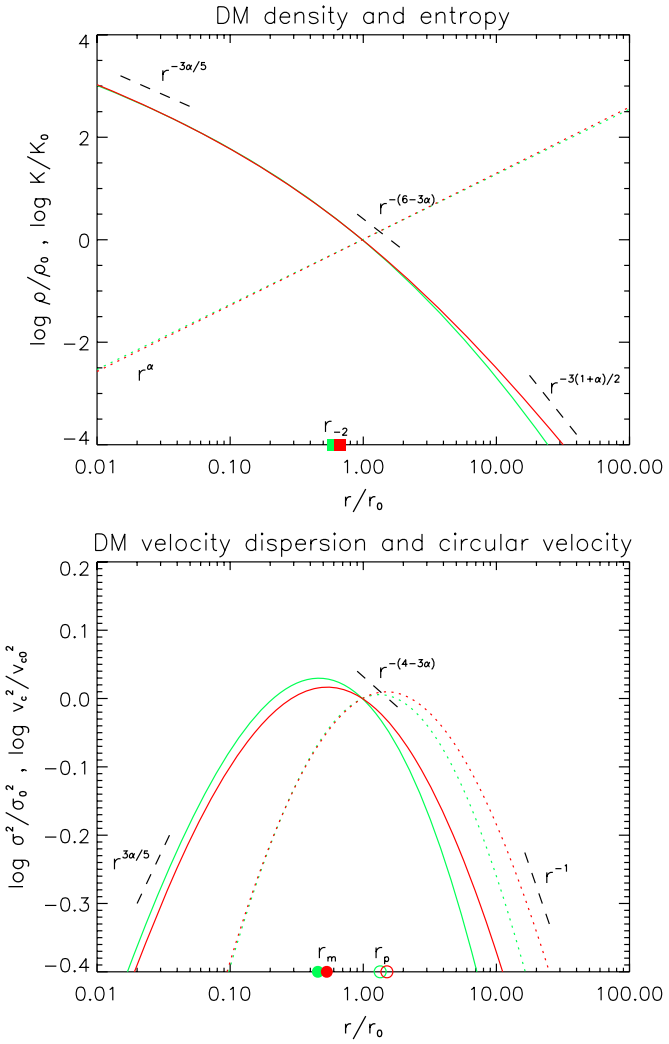

Figure 1. Top panel: radial runs of the DM density (solid) and entropy (dotted); bottom panel: radial runs of the DM velocity dispersion (solid) and circular velocity (dotted). Both panels refer to the α-profiles with $\alpha = 1.27$ (green lines) and $\alpha = 1.3$ (red lines); the profiles are normalized to unity at the radius r_0 where the density slope γ_0 applies. The behaviors in the inner regions, main body, and outskirts are highlighted by black dashed lines. The radii r_{-2} where the density slopes equal -2 (used in defining the concentration c, see Section 2), r_m, the velocity dispersion peak, and r_p, the circular velocity peak, are highlighted as squares, filled circles, and empty circles, respectively.

(A color version of this figure is available in the online journal.)

from the central rise of $K(r)$ and the outer steep falloff of $\rho(r)$, and will have a striking counterpart in the ICP. The characteristic values of σ^2 for the α-profiles are set in terms of *minimal* values for $\sigma^2 = v_c^2/\kappa_{\rm crit}$; this is related to limited randomization during accretion of the infall kinetic energy gained by the initially cold DM particles.

These α-profiles actually depend weakly on α in the named range (see Figure 1), and though derived from the isotropic Jeans Equation (3) prove to be *stable* against the addition of reasonable anisotropies. The latter are described by the standard Binney (1978) parameter $\hat{\beta}$, whose numerical simulations suggest to increase outward from central values $\hat{\beta}(0) \gtrsim -0.1$ meaning weakly tangential anisotropy, toward $\hat{\beta} \lesssim 0.5$ that implies prevailing radial motions (see Dehnen & McLaughlin 2005; Hansen & Moore 2006; also Høst et al. 2009). Such density profiles turn out to be slightly *flattened* at the center and considerably *steepened* into the outskirts.

The α-profiles are also *stable* against educated variations in the condition $\alpha = \text{const}$. Actually, the cosmogonic buildup given by our semianalytic computation yields a slow decrease of $\alpha(r)$ into the outskirts, as these develop from the inside out at late times after the transition. Again in keeping with the simulations, the outer development does not affect the inner gravitational potential and the equilibrium described by the Jeans equation, which (with its central boundary condition) also works from the inside out. In fact, for the present use we have computed the density profiles associated with $\alpha(r)$, and checked these to be very close to the parent α-profiles but for being somewhat steeper into the outskirts, with densities lower by about 15% in the vicinity of the virial radius.

It is to be stressed that the α-profiles for $M \sim 10^{14}$–$10^{15}\, M_\odot$, especially with full $\alpha(r)$ and anisotropies, turn out to provide an optimal fit to the surface density runs as derived from gravitational lensing observations in around massive clusters that just require central slopes flatter and outer slopes steeper than the standard NFW (e.g., Broadhurst et al. 2008). Such a fit for A1689 requires high values $c \sim 10$ and early transition epochs $z_t \approx 1.5$, related conditions that the two-stage development predicts to occur in about 10% of the rich clusters (Lapi & Cavaliere 2009b).

We will adopt these α-profiles depending on the *two* DM key parameters α and c to describe the gravitational potential containing the ICP, to which we now turn.

3. THE ICP EQUILIBRIUM

We will focus on clusters in equilibrium conditions, in between the punctuating violent mergers for which we refer the reader to the review by Markevitch & Vikhlinin (2007). When the DM halo is close to equilibrium, even more so will be the pervading ICP; in fact, the sound crossing time $R/(5\,k_{\rm B}T/3\,\mu m_p)^{1/2}$ is seen to be somewhat shorter than the dynamical time R/σ on recalling from Section 1 that $k_{\rm B}T \approx \mu m_p\,\sigma^2$ holds. In these conditions, the ICP is governed by the hydrostatic, Jeans-like equation provided by the first and the second member of Equation (2). In a compact form similar to Equation (3), this writes

$$g = \tfrac{3}{5}\,a + \tfrac{3}{5}\,b, \tag{7}$$

once the ICP entropy run $k(r)$ is given and used to factor out the product $d\,(k\,n^{5/3})/dr$ in the original Equation (2). In fact, the entropy slope $a \equiv d\log k/d\log r$ enters Equation (7) to yield the running density slope $g(r) \equiv -d\log n/d\log r$, concurring with the gravitational pull measured by the (squared) ratio $3\,b(r)/5 \equiv 3\,\mu m_p\,v_c^2(r)/5\,k_{\rm B}T(r)$ of the DM circular velocity (discussed in Section 2) to the sound speed.

The above constitutes just a first-order differential equation that transforms to linear in terms of the variable $n^{2/3}(r)$. By textbook recipes (e.g., Dwight 1961) this is amenable to a simple solution in form of a quadrature that is conveniently written as

$$\begin{aligned}\bar{T}(\bar{r}) &= \bar{k}(\bar{r})\,\bar{n}^{2/3}(\bar{r}) \\ &= \bar{k}^{\,3/5}(\bar{r})\left[1 + \frac{2}{5}\,b_R\int_{\bar{r}}^{1}\frac{d\bar{r}'}{\bar{r}'}\,\bar{v}_c^2(\bar{r}')\,\bar{k}^{-3/5}(\bar{r}')\right];\end{aligned} \tag{8}$$

here barred variables are normalized to their boundary value at $r = R$, where $b(r)$ takes on the value b_R, while $v_c^2(r)$ is taken from the α-profiles with its weak dependence on α.

To illustrate the content of Equation (8), in Figure 2 (top panel) we plot the integral basing on the run $k(r)$ given in Equation (17), along with the simple analytical fit presented in Appendix A. Note two circumstances: (1) $2\,b_R/5 \approx 1$ holds (e.g., $2\,b_R/5 \approx 1.06$–1.02 on using $b_R = 2.65$–2.55, see Equation (10)); (2) on approaching the center the integral dominates in the square bracket, thus the memory of the boundary condition is swamped and the whole square bracket is numerically found to scale as $k_c^{-1/4}$ with the central entropy k_c, see Figure 2 (bottom panel). Note that where the r-dependence of the bracket saturates, Equation (8) implies $T(r) \propto n^{-1}(r) \propto k^{3/5}(r)$.

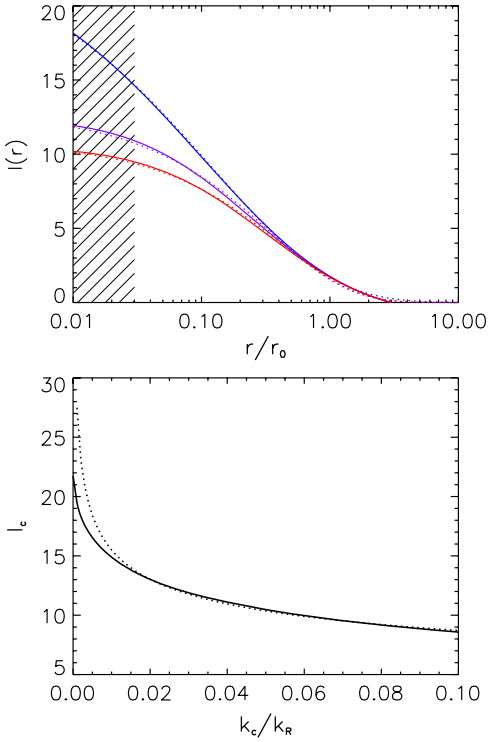

Figure 2. Top panel: the integral entering Equation (8) is plotted as a function of r for the values $\bar{k}_c = 5\times10^{-2}$ (red), 2.5×10^{-2} (cyan), and 0 (blue) used in the next figures; the dotted lines represent the analytic fit provided in Appendix A. Bottom panel: the value of the integral at the center is plotted as a function of $\bar{k}_c$ (solid line), and is compared with the power-law approximation $\bar{k}_c^{-1/4}$ (dotted line); the latter holds to better than 5% in the most relevant range $\bar{k}_c \approx 0.01$–0.15, see Section 4.

(A color version of this figure is available in the online journal.)

The issue to stress is that, rather than a model, the above Equation (8) has the standing of a *theorem* in hydrostatics valid for clusters close to equilibrium.

3.1. ICP Entropy

What actually needs *physical* discussion and modeling is the entropy run $k(r)$. We base on the notions that entropy is erased by radiative cooling on the timescale $t_c \approx 65\,(k_{\rm B}T/5\,{\rm keV})^{1/2}\,(n/10^{-3}\,{\rm cm}^{-3})^{-1}$ Gyr (Sarazin 1988), while substantial raising requires *shocks* (see Appendix B) as are driven by supersonic outflows from center and set by inflows across the boundary.

3.1.1. Entropy Deposited at the Boundary

At the outer end, the mathematics of Equation (7) requires one boundary condition fixing b_R. On the observational side, $T(r)$ is found to decline slowly toward the virial radius (Molendi & Pizzolato 2001), and at such a rate it would take tens of Mpc to decline smoothly from keV values to those some 10^{-2} times lower as prevailing in the external medium. So at $r \approx R$ a

discontinuity is to occur and terminate the hot ICP, at variance with the smooth if steeper decline of the DM density. In fact, most of the transition takes place across a few mean free paths λ_{pp} at the *accretion shocks* produced when external gas supersonically falls into the DM potential.

Numerical simulations (e.g., Tormen et al. 2004, see their Figure 8) show that accretion of the smooth gas and minor lumps making up a major fraction of the accreted mass drives a complex patchwork of shocks mostly comprised within an outer layer with thickness of order $10^{-1}\,R$; across such a layer the standard conservation laws of mass, momentum, and energy may be applied leading to the classic Rankine–Hugoniot jump conditions; to within 10% the results are similar to a coherent accretion shock, roughly spherical and located at $r \sim R$ (see LCM05 for a complete treatment, and Ettori & Fabian 1998 for possibly delayed electron equilibrium). The impact of major lumps reaching down to the center will be dealt with in Section 3.1.3.

The jump conditions take on a particularly simple form for cold inflow into rich clusters that cause *strong* shocks with Mach numbers squared $\mathcal{M}^2$ considerably exceeding unity (see Appendix B). In strong shocks lingering at $r \approx R$ (and expanding along with the cluster's development), maximal conversion of infall energy occurs over a radial range of order λ_{pp} to yield

$$k_B T_R = \tfrac{2}{3}\,\mu m_p\, v_R^2\,\Delta\phi_{tR}, \tag{9}$$

where $2v_R^2\,\Delta\phi_{tR}$ is the kinetic energy per unit mass of the gas freely falling across the potential drop down to $r = R$ from the turning point where infall starts (see LCM05). Thus, we find

$$b_R = \frac{3}{2\,\Delta\phi_{tR}}, \tag{10}$$

with values 2.65–2.55 corresponding to $\alpha = 1.27$–1.3 and $\Delta\phi_{tR} \approx 0.57$–$0.59$.

At the boundary the equilibrium, Equation (7) yields $g = 3\,(a + b_R)/5$. Meanwhile, power-law approximations $k \propto r^a$, $n \propto r^{-g}$ apply in the vicinity of $r = R$, so $m(r) \propto r^{3-g}$ describes the ICP mass m in the outer layer, and correspondingly

$$k \propto m^{a/(3-g)} \propto m^{5a/3(5-a-b_R)} \tag{11}$$

obtains.

On the other hand, pursuing the scaling for $K(r)$ recalled in Section 2, LC09 show that the DM entropy behaves as $K \propto M^{4/3}/M^{2/3} \propto M^{3/2}$ on considering that $M \propto t^{4/5}$ holds in the standard ΛCDM cosmogony for $z \lesssim 0.5$ during the slow accretion stage. As external gas and DM are accreted in cosmic proportion, in the outer layer $\dot{m} \propto \dot{M}$ applies, and it follows that the ICP entropy at the boundary can be expressed as

$$k \propto m^{3/2}. \tag{12}$$

Then, on equating the exponents in Equations (11) and (12) one finds

$$a_R = \frac{45 - 9\,b_R}{19} \quad \text{and} \quad g_R = \frac{27 + 6\,b_R}{19}. \tag{13}$$

With the values of b_R discussed above, these yield the slopes $a_R \approx 1.1$ and $g_R \approx 2.2$, both considerably *flatter* than the corresponding DM values. Note from Equation (13) how the slope a_R at the boundary decreases if b_R is increased. We expect such a decrease to take place for clusters with high concentrations corresponding to shallow outer potentials (see Lapi & Cavaliere 2009b) that decrease the outer drops $\Delta\phi_{tR}$ entering b_R through Equation (10). For example, a value $c \approx 10$ (holding for a cluster with an early transition, see Section 2) in place of the usual $c \approx 4$ (holding for clusters with a recent transition) implies $\Delta\phi_{tR}$ to lower to 0.47, b_R to grow to 3.2, and a_R to decrease to 0.85 as may be the case for A1689 (see Lemze et al. 2008; Lapi & Cavaliere 2009b); meanwhile, from Equation (13) g_R increases to 2.4. A flat entropy slope may be also produced when the boundary shock is weakened by substantial preheating of the infalling gas; such a condition is relevant for poor clusters and groups with comparatively low potentials (see LCM05), e.g., $a \approx 0.8$ applies to systems with $M \lesssim 10^{14}\,M_\odot$ with external preheating at levels around 1/2 keV per particle.

On the other hand, after Equation (13) high values of a with an upper bound at $45/19 \approx 2.4$ (in keeping with the variance observed by Cavagnolo et al. 2009) correspond to low values of b_R, hence to large $\Delta\phi_{tR}$; these imply flat densities and temperatures sustained to high values in the outskirts.

3.1.2. Entropy Stratification

No other major sources or sinks of energy and entropy occur inward of the boundary at a few Mpc down to the central 10^2 kpc. So throughout the ICP bulk, the entropy slope is to stay at its boundary value $a = a_R$, and in rich clusters with standard concentration

$$k(r) \propto r^{1.1} \tag{14}$$

is to hold, a result similar to Tozzi & Norman (2001), LCM05, and Voit (2005).

On the other hand, while the simple thermodynamics of the ICP maintains the run of $k(r)$ in this power-law form, its more complex adiabatic readjustments within the gravitational well cause the density slope $g(r)$ to flatten out inward; this is granted by Equation (7), as the inequality $b(r) < b_R$ (i.e., $v_c^2(r)/k_B T(r) < 1$) progressively strengthens away from the boundary. As a result, the ICP slope $g(r)$ not only starts out but also stays generally *flatter* than DM's $\gamma(r)$ inward of the boundary, as given by

$$g(r) = 3\,[a + b(r)]/5 < 3\,[\alpha + \kappa(r)]/5 = \gamma(r). \tag{15}$$

This implies the ICP density run $n(r)$ at the boundary to parallel the DM's $\rho(r)$ at some other point well inside the cluster's main body.

3.1.3. Entropy in the Central Region

Next, we discuss the central value k_c of the entropy and its origins. Recall from Section 1 that the central entropy may be produced by shocks driven by substantial merging events reaching the center (McCarthy et al. 2007; Balogh et al. 2007), and by AGNs residing in the central bulge-dominated galaxies (see Valageas & Silk 1999; Wu et al. 2000; Cavaliere et al. 2002; Scannapieco & Oh 2004; LCM05). In addition, a basal entropy level may be left over by SNe and AGNs that preheated the gas in the volume due to collapse into, or to accretion onto the cluster (LCM05; McCarthy et al. 2008).

To begin with, consider preheating; this may be expressed in terms of entropy advected across the shock by the currently infalling gas (see Appendix B). However, such a process is known to be effective only within limits: if always strong, it would flatten the bulk entropy slope of most clusters to values

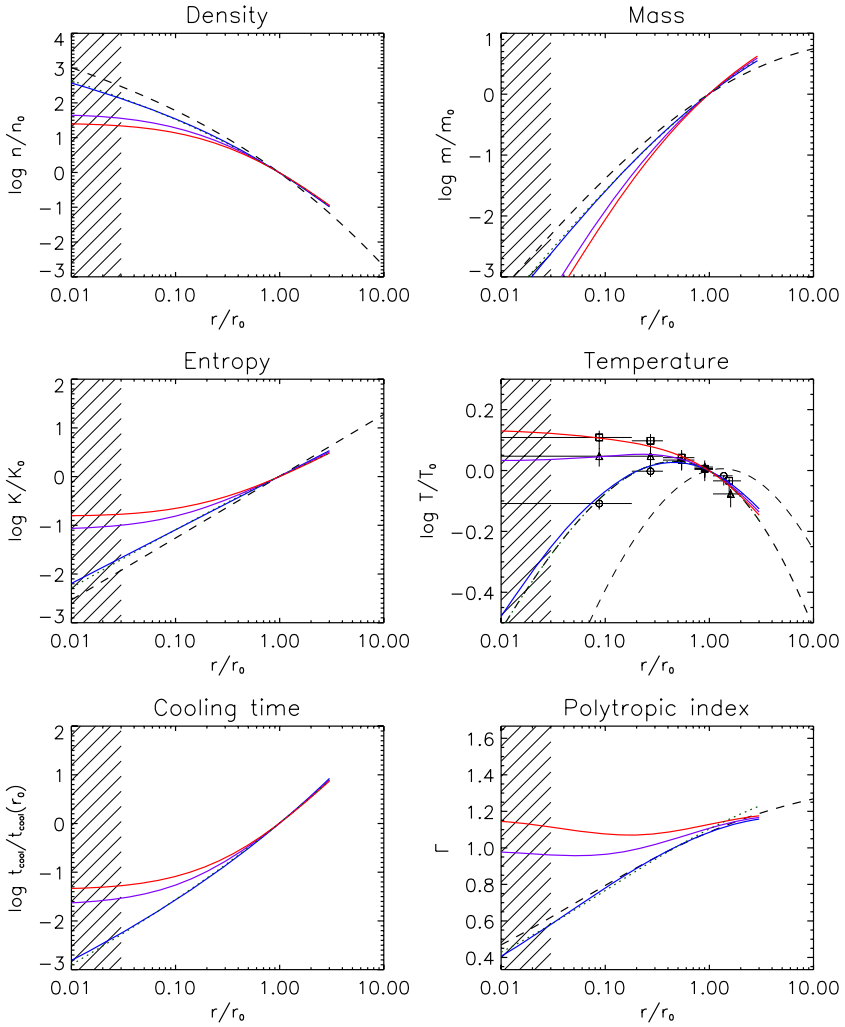

Figure 3. Radial runs of the ICP density, mass, entropy, temperature, cooling time, and polytropic index given by the Supermodel. The solid lines are for different values of the central entropy $\bar{k}_c = 5 \times 10^{-2}$ (red), 2.5×10^{-2} (cyan), and 0 (blue); the dotted lines refer to the "mirror" model discussed in Section 6.1 with $\beta = 0.75$; the dashed lines illustrate the underlying DM distribution taken from the α-profile with $\alpha = 1.27$ and an average concentration value $c \equiv R/r_{-2} = 5$ (see Section 2). In the panel representing $T(r)$, we plot the DM velocity dispersion $\sigma^2(r)$ as a thick dashed line, and the circular velocity $v_c^2(r)$ as a thin dashed line; we also show average data for the CC (circles), NCC (squares), and UNC (triangles) classes from Leccardi & Molendi (2008). The hatched area outlines the central range hardly accessible to current resolutions.

(A color version of this figure is available in the online journal.)

$a < 1$ (see Section 3.1.1 and Figure 3), and produce really flat entropy profiles in most groups at variance with the observations (see Balogh et al. 1999; Pratt & Arnaud 2003; Rasmussen & Ponman 2004); unless tailored to cluster precollapse size, it would involve larger volumes and require high total energetics; finally, the presence of Lyα absorbers limits actual preheating to optimal redshifts $z \sim 2$–3 when it may catch the peak of star/AGN formation while still operating at moderate cosmological densities (see Voit 2005).

Consider then the shocks produced at cluster centers by major mergers. A main progenitor with mass already close to the present value M undergoes only a few more, if any, merging shocks; each of these, in view of the considerable mass import and high-infall velocity, can deliver large energies up to 10^{64} erg or several keV per particle, and may produce levels of k_c up to several 10^2 keV cm^2 (see Appendix B). With timescales for free radiative cooling of order

$$t_c \approx 0.3 \left(\frac{k_c}{15\,\mathrm{keV\,cm^2}}\right)^{3/2} \left(\frac{k_\mathrm{B}T}{5\,\mathrm{keV}}\right)^{-1} \mathrm{Gyr}, \qquad (16)$$

(Voit & Donahue 2005), the above levels take several Gyr to decrease substantially. At the other end, a much lower entropy state would rapidly run down to values lower still. So a key point is to secure intermediate but persisting entropy levels.

Values of k_c in the range 10–30 keV cm^2 as frequently observed despite fast radiative erasure point toward entropy inputs frequently refreshed; a promising path is provided by sizeable and recurrent energy injections by central AGNs, triggered into activity by renewed fueling in a low-entropy, dense environment of their underlying supermassive black holes (BHs). These are observed to undergo outbursts able to inject, nearly independent of cluster mass, energies ΔE up to 10^{62} erg or a few keV per particle, yielding k_c of several tens keV cm^2. Cooling on the scale of 10^{-1} Gyr may be offset as the several supermassive BHs inhabiting the many bulge-dominated galaxies in the central region of a rich cluster alternatively kindle up, and collectively recur over such timescales (see Nusser et al. 2006; Ciotti & Ostriker 2007; Conroy & Ostriker 2008). In particular, outbursts lasting for a few 10^8 yr can continuously drive out to 300 kpc pressurized blast waves terminating into a

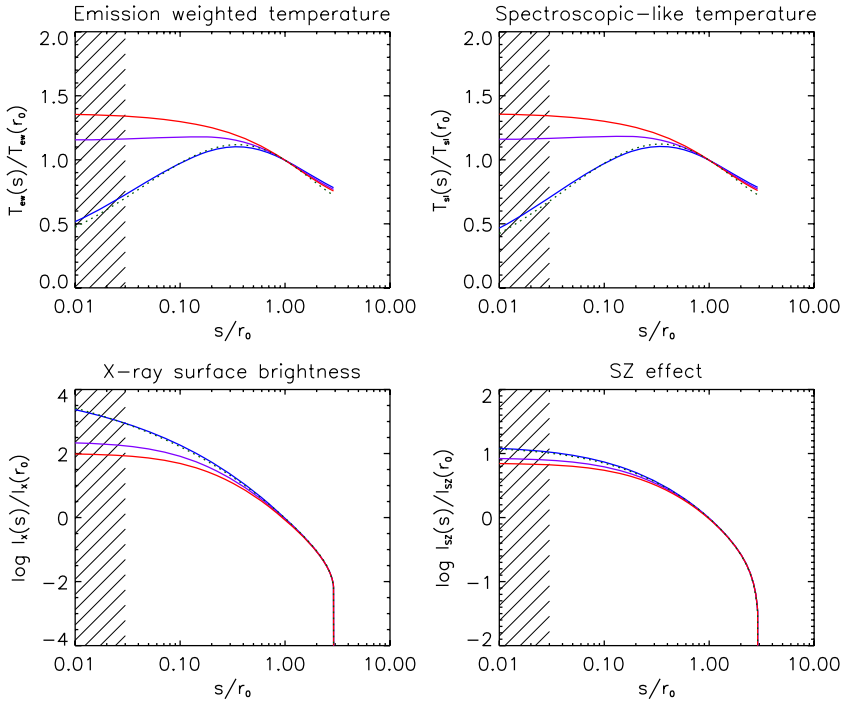

Figure 4. ICP-projected distributions of emission-weighted temperature, spectroscopic-like temperature, X-ray surface brightness, and l.o.s. SZ effect. Line styles as in Figure 3.

(A color version of this figure is available in the online journal.)

shock with Mach numbers sustained at $\mathcal{M}^2 \gtrsim 3$, as computed in detail by LCM05 and observed by Forman et al. (2005), Nulsen et al. (2005), and McNamara & Nulsen (2007), see also Appendix B.

All these processes contribute to raise the entropy over an extended region around the center, adding to the outer run given by Equation (14); the combined entropy profile may be described by the simple parametric expression (see Voit 2005 and references therein)

$$\bar{k}(\bar{r}) = \bar{k}_c + (1 - \bar{k}_c)\,\bar{r}^a \tag{17}$$

represented in Figure 3. Having computed the outer power-law slope a around 1.1 (see Section 3.1.1) and having discussed central entropy levels k_c from a few tens to several hundreds keV cm^2, we next use these *two* ICP key parameters in our equilibrium "Supermodel."

4. THE SUPERMODEL FOR CC AND NCC CLUSTERS

The run of $k(r)$ in the handy form Equation (17) may be inserted into the hydrostatic equilibrium Equation (8) to yield the *Supermodel* for the ICP disposition. Away from the boundary this links $T(r)$ and $n(r)$ *inversely*; such an inverse link is particularly clear at the very center, as is seen from the dependencies $T_c(k_c)$ and $n_c(k_c)$ obtained from Equation (8) on considering the explicit scalings $T_c \propto k_c^{3/5}$ and $n_c \propto k_c^{-3/5}$ with the further factor supplied by the dominant integral that scales as $k_c^{-0.25}$ (see Appendix A). Thus, the overall scaling laws read

$$T_c \propto k_c^{0.35}, n_c \propto k_c^{-1}; \tag{18}$$

these yield $T_c \propto n_c^{-0.35}$, from which we see clearly how low/high T_c correspond to high/low n_c. In addition, it is easily perceived, and is seen from Figure 3, that the central runs of $n(r)$ are angled or core-like, depending on k_c being low or high.

There is much more. Figure 3 shows that the Supermodel provides simultaneous, *accurate* descriptions to both the *full* profiles of $T(r)$ as directly given by Equation (8) and of the surface brightness in X rays provided on integrating along the l.o.s., the volume emissivity for optically thin thermal bremsstrahlung; this reads $2.4 \times 10^{-27}\,\mathcal{L}_X$ erg s^{-1} cm^{-3} with $\mathcal{L}_X \propto n^2\,T^{1/2}$ (emission lines add for $k_{\rm B}T \lesssim 2$ keV; see Sarazin 1988). After Equation (8) one has

$$\mathcal{L}_X(\bar{r}) \propto \bar{k}^{-9/10}(\bar{r}) \left[1 + 2/5\, b_R \int_{\bar{r}}^{1} d\bar{r}'\bar{k}^{-3/5}(\bar{r}')\,\bar{v}_c^2(\bar{r}')/\bar{r}'\right]^{7/2}, \tag{19}$$

with the central scaling given by $\mathcal{L}_X(0) \propto k_c^{-1.8}$. These profiles depend strongly on the value of k_c that primarily governs the central pressure and hence the central density run (see Figure 3); weakly on a (and b_R) that governs the middle run; and mildly on the DM concentration c (see Section 2) that governs the outer decline toward the boundary values.

We illustrate in Figures 3 and 4 how straightforwardly the Supermodel describes various observables for both classes of CC and NCC clusters as identified by Leccardi & Molendi (2008), and also for their intermediate class of UNC clusters. In Figures 5–7, we focus on the specific cases of the clusters A2218, A2204, and A1413 for which both high-resolution *XMM-Newton* and preliminary *Suzaku* data are available.

From these results is clearly seen how CC clusters are marked out by the presence of a *peak* of $T(r)$ at $r \approx 0.1$–$0.2\,R$ (or equivalently by $T_c < T_R$). The condition for the peak to occur is highlighted on recalling from Equation (8) that

$$T(r) \propto k(r)\,n^{2/3}(r) \tag{20}$$

applies as the ICP counterpart of Equation (6) for the DM. Given that $n(r)$ rises monotonically inward, $T(r)$ will peak and then decline toward the center when $k^{3/5}(r)$ decreases strongly

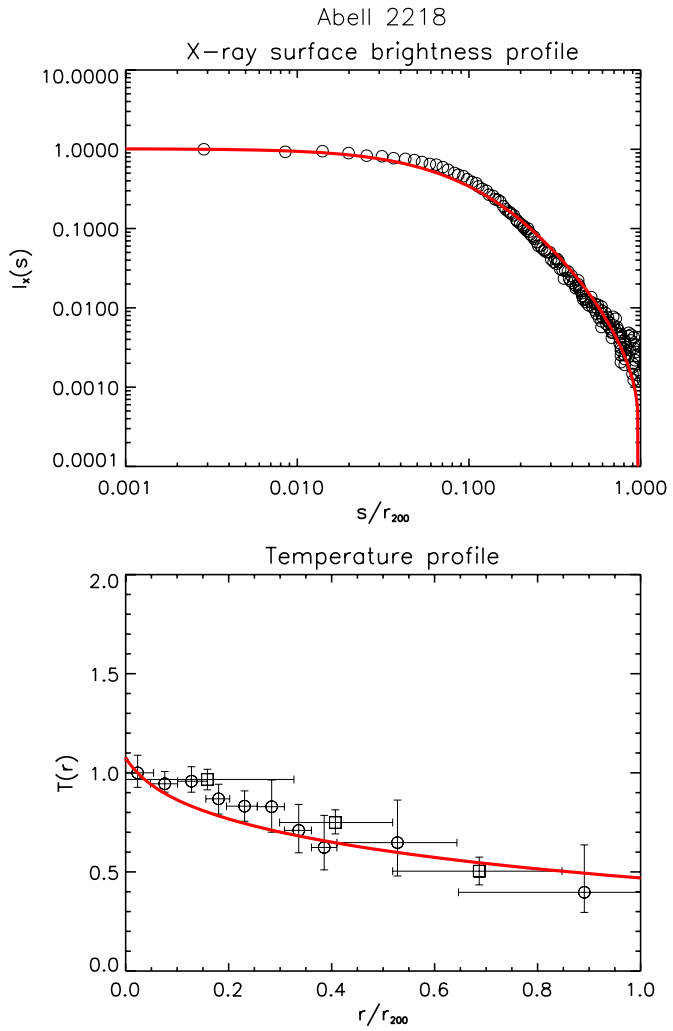

Figure 5. X-ray surface brightness and temperature of the NCC cluster A2218. The circles represent *XMM-Newton* data (Zhang et al. 2008), while squares refer to preliminary *Suzaku* observations. For the sake of clarity, in the top panel we do not report the formal error bars; these are generally small, except for the outermost data limited by sensitivity, and for the innermost ones limited by resolution. The solid line represents the Supermodel for a given DM $\alpha = 1.27$ profile with concentration $c = 3.5$, and ICP entropy with slope $a = 1.1$ and central value $\bar{k}_c = 10^{-1}$.

(A color version of this figure is available in the online journal.)

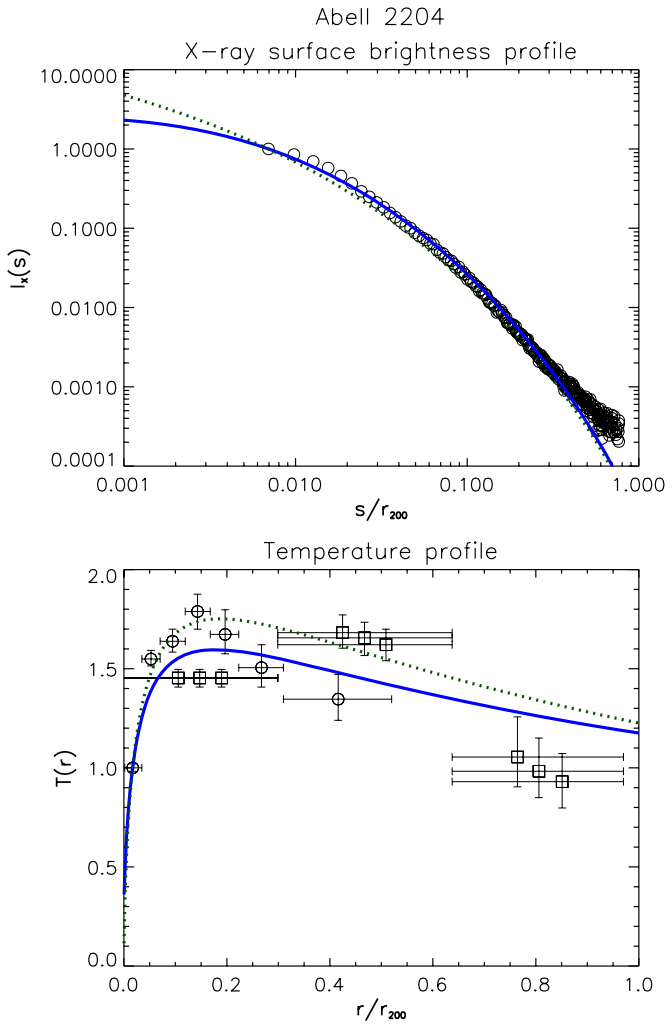

Figure 6. Same as in Figure 5 for the CC cluster A2204. The solid line represents the Supermodel for a given DM $\alpha = 1.27$ profile with concentration $c = 4$, and ICP entropy with slope $a = 1.1$ and central value $\bar{k}_c = 10^{-3}$. The dotted line refers to the approximation presented in Section 6.1.

(A color version of this figure is available in the online journal.)

toward a low value of k_c, as is the case with the CC clusters. On the other hand, $T(r)$ will rise to a central, roughly isothermal *plateau* for sufficiently high values of k_c.

From the condition for a maximum to occur in the functional form of $T(r)$ as given by Equation (8), on using $v_c^2(r)$ from the α-profiles with $\alpha = 1.27$–1.3 the threshold value for the peak reads

$$\bar{k}_c \approx 2.5 \times 10^{-2}; \tag{21}$$

with boundary values $k_R \approx 1500$–2000 keV cm^2, these correspond to $k_c \approx 40$–50 keV cm^2. In closer detail, the peak looms out (the case of UNC clusters) for $\bar{k}_c \approx 2.5 \times 10^{-2}$, and stands out (the case of CC clusters) for $\bar{k}_c \lesssim 10^{-2}$ corresponding to $k_c \approx 15$–20 keV cm^2.

We stress that a *finite* $T_c \neq 0$ constitutes a natural feature of the equilibrium for CC clusters rather than some peculiarity of cooling flows (see discussion by Peterson & Fabian 2006). This holds with realistically small values of k_c; but even if k_c were formally null, T_c would decline toward the very center with a somewhat flatter power law $r^{3a/5}$ compared to $\sigma^2 \propto r^{3\alpha/5}$. This behavior is consistent with the nonradiative runs of the hydrodynamical simulations by Borgani (2007, see his Figure 1).

A feature typical of the Supermodel is the peak of $T(r)$ closely following the maximum of the DM velocity *dispersion* $\sigma^2(r)$, not that of the circular velocity $v_c^2(r)$, see Figure 3 (middle right panel). As the former moves considerably downward with masses ranging from 10^{15} to $10^{13}\ M_\odot$ (see Figure 1 and LC09), we predict the peak of $T(r)$ should also *move* to progressively lower radii in going from rich to poor clusters and groups; preliminary data by Nagai et al. (2007) support the prediction, but robust data require secure *Chandra* calibrations.

Finally, the Comptonization parameter for the SZ effect (Sunyaev & Zel'dovich 1972) obtains from integrating along an l.o.s. the volume quantity $\mathcal{Y} \propto p$ in terms of the (thermalized) electron pressure $p = n\, k_B T$; after Equation (8) this means

$$\mathcal{Y}(\bar{r}) \propto \left[1 + 2/5\, b_R \int_{\bar{r}}^{1} d\bar{r}'\bar{k}^{-3/5}(\bar{r}')\, \bar{v}_c^2(\bar{r}')/\bar{r}'\right]^{5/2}, \tag{22}$$

to the result plotted in Figure 4. In the central region, this scales as $\mathcal{Y}(0) \propto \bar{k}_c^{-0.65}$.

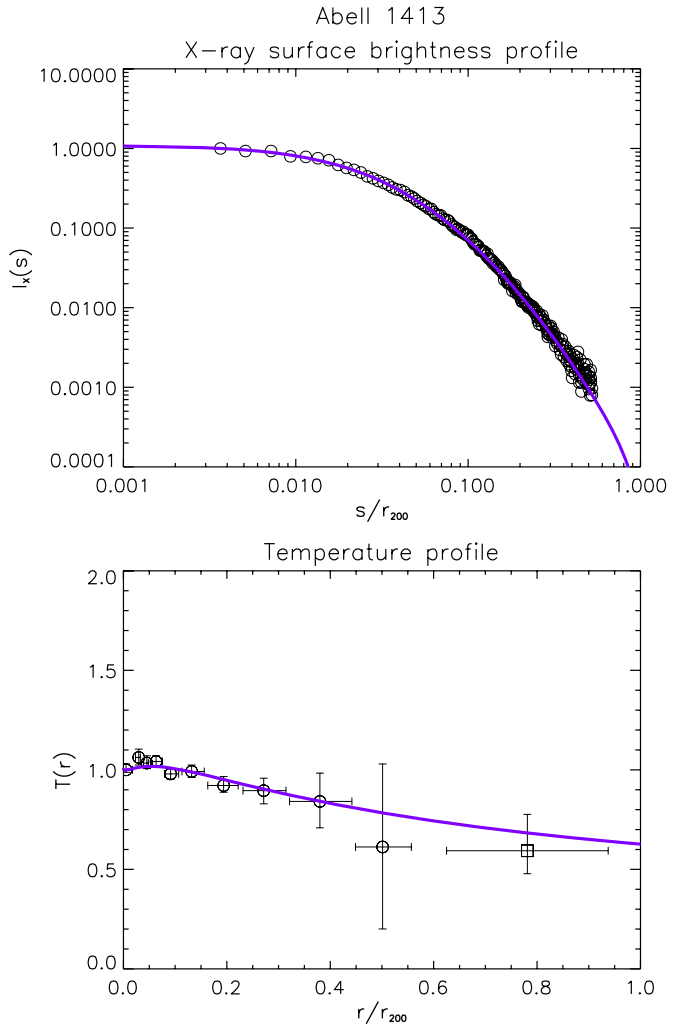

Figure 7. Same as in Figure 5 for the UNC cluster A1413. The solid line represents the Supermodel for a given DM $\alpha = 1.27$ profile with concentration $c = 5.5$, and ICP entropy with slope $a = 1.1$ and central value $\bar{k}_c = 2.5 \times 10^{-2}$. (A color version of this figure is available in the online journal.)

5. STABILITY OF THE CENTRAL CONDITIONS

Having shown how the Supermodel focuses the central conditions, here we pursue the discussion ending Section 3, and argue that they are robust against energy losses or additions.

5.1. From Cool Cores to Cooling Cores, and Back

Clearly, the CC state produced by the Supermodel differs not only from a cooling flow but also from a freely cooling core; in fact, cooling is not included in Equation (7) as it stands. However, the Supermodel focuses the conditions for enhanced radiation and fast cooling to set in, namely, low though *finite* $T_c \propto k_c^{0.35}$ *linked* to high n_c so as to imply

$$t_c \approx 0.3 \left(\frac{k_c}{15\,\mathrm{keV\,cm^2}} \right)^{1.2} \mathrm{Gyr}. \qquad (23)$$

Figure 3 (bottom left panel) illustrates the run $t_c(r)$ of the cooling time throughout a CC cluster.

The above concerns the Supermodel proper. The sequel of the story is long accepted, in general terms, to imply that such an enhanced radiation will lead to entropy loss, which in turn will further lower T_c and increase n_c, so shortening t_c and opening the way for a classic cooling catastrophe to set in (White & Rees 1978; Blanchard et al. 1992). A possible happy ending to the cooling story in clusters has been widely proposed and discussed (see Binney & Tabor 1995; Cavaliere et al. 2002; Voit & Donahue 2005; Ciotti & Ostriker 2001; Tucker et al. 2007), to the effect that, before the conditions run away into a full catastrophe, the ICP condensing around central massive galaxies and mixing with their ISM is very likely to kindle AGN activities by renewing mass accretion onto their powerhouses, the supermassive BHs lurking and starving at most galactic centers. Thus, recurrent loops are conceivably started by cooling that rekindles AGNs that in turn feed back energy into the surrounding medium to eventually quench the BH accretion flow and ultimately yield quasi-steady, widespread conditions with k_c reset over timescales of some 10^8 yr to values around 15 keV cm^2.

5.2. Saturation in Non-cool Cores

On the other hand, NCC conditions prevail above the divide at $k_c \approx 40$–50 keV cm^2. We understand the fewer NCC relative to the CC clusters primarily on the basis of strong AGN inputs, in the tail of the AGN luminosity function $N(L)$ (e.g., Richards et al. 2006); this implies for the output statistics $\Delta E\, N(\Delta E) \propto L\, N(L)$ a sharp decline above $\Delta E \approx 5 \times 10^{61}$ erg. We also note that hotter cluster centers tend to impair or prevent the supersonic condition necessary for driving strong pressurized blast waves (see Appendix B), i.e., $\mathcal{M}^2 \approx 1 - \Delta E/E \gtrsim 3$ corresponding to $\Delta E/2\, k_B T_c\, m \gtrsim 1$; meanwhile the entropy deposited reads $k_c \approx \Delta E/(1 - \Delta E/2E)^{2/3}$. This will saturate the effects of multiple inputs, if any, occurring within a cooling time.

Similar arguments also apply to the possibly larger if generally rarer energy outputs associated with substantial mergers; these may be up to $\Delta E \lesssim 10^{64}$ erg (see Section 3.1.3), but by the same token the energies effectively transferred to the ICP in NCC conditions are especially prone to saturate after the first such event.

5.3. Concluding on Central Conditions

Taking up from Section 3.1.3, we recall that the cooling-fueling feedback machinery calls for a correlation between CC clusters and current central AGNs (the so-called dichotomy, see Voit 2005) that finds support from a considerable body of observations (e.g., Mittal et al. 2009). This picture is currently under scrutiny in study cases such as provided by the poor cluster AWM4; there the considerable value $k_c \approx 60$ keV cm^2 calls for a fueling process unrelated to cooling, with energetics higher than implied by the current radio activity. In addition, no signatures or fossil imprints have yet been found of large energy inputs caused over the past 10^{-1} Gyr by either major AGN outbursts or mergers (Gastaldello et al. 2008; Giacintucci et al. 2008). This may constitute as of today one instance of an exceptional preheating level, standing out as a main component to k_c.

To complete the picture, AGNs as widespread agencies for raising the central entropies lead to an understanding of the steep decline of the local L_X–T correlation from clusters to groups, or the equivalent saturation in groups of the k–T correlation (see Ponman et al. 2003; Pratt et al. 2009), in terms of comparable single outbursts in differently sized galaxy systems (Cavaliere et al. 2002; LCM05). Finally, AGN kinetic plus radiative outputs also lead to the expection of a nonmonotonic rise and fall of

the relation L_X–z, consistent with the current data for clusters (Cavaliere & Lapi 2008).

In sum, the two main modes for energy injections, namely central AGNs and major mergers, provide different levels of entropy input; whence we expect a bimodal distribution for the observed number of clusters as a function of the central entropy level k_c. In fact, the two peaks should be remolded to an actual distance considerably smaller than the factor 10^2 separating the two maximal input levels; this is because the statistics will be eroded at low k_c by fast cooling, while limited at high k_c by the small number of strong input events. The expected outcome will be not unlike the findings recently presented by Voit (2008) and Cavagnolo et al. (2009).

We conclude that both the CC and the NCC central conditions envisaged by the Supermodel are made *robust* by processes additional but naturally geared to it.

6. LIMITING MODELS

While the Supermodel can yield accurate representations of the ICP state with a moderate amount of formalism, it is nevertheless worthwhile to have handy limiting models for prompt interpretations and predictions of data.

6.1. Mirror Dispersions

We take up the point made in Section 4 as to $T(r)$ following $\sigma^2(r)$ for CC clusters, and show in Figures 3 (middle right) and 6 (bottom panel) the good performance around the $T(r)$ peak and shortward (but for the very central range where $T(r)$ deviates upward to its value $T_c \propto k_c^{0.35}$) provided by the simple model with the ICP mirroring the DM dispersion

$$T = \sigma^2/\beta. \tag{24}$$

The normalizations are included in the constant parameter $\beta \equiv \mu m_p \sigma^2/k_B T$ that in Figure 6 is fixed at 0.75, just the natural value it takes when evaluated at R.

This is similar to the approximation discussed by Cavaliere & Fusco-Femiano (1981) and tested by Hansen & Piffaretti (2007), and similarly yields the density in the explicit form

$$\bar{n}(\bar{r}) = \bar{\rho}^{\beta}(\bar{r})\,\bar{\sigma}^{2(\beta-1)}(\bar{r}). \tag{25}$$

Here, the DM density $\rho(r)$ is provided by the α-profiles of Section 2, to imply

$$n(r) \propto r^{\alpha(\beta-1)}\,\rho^{5\beta/3-2/3}(r), \tag{26}$$

which goes into the simple form $n(r) \propto \rho(r)$ toward the center in the range where $\rho(r) \to r^{3\alpha/5}$ holds but still Equation (25) applies.

6.2. Polytropic β-Models

For NCC clusters, instead, we make contact with the classic β-models discussed by Cavaliere & Fusco-Femiano (1978).

In the central region, the contact obtains from noting these clusters to be marked by high values of k_c that cause a nearly flat central run of the entropy after Equation (17). It is now a matter of straightforward algebra to see that on taking $k(r) \approx k_c$ to a zeroth approximation, this may be extracted from the integral in Equation (8) to yield directly

$$T/T_c = (n/n_c)^{2/3} = 1 + 2\,\beta_c\,\Delta\phi_{c,r}/5 \tag{27}$$

corresponding to a polytropic approximation with macroscopic index $\Gamma \equiv 5/3 + d\log k/d\log n = 5/3$. To a next approximation, Γ may be obtained by carrying further the expansion of the integral to obtain

$$\Gamma \simeq \frac{5}{3}\left[1 - \frac{2}{5}\,\frac{1-\bar{k}_c}{\bar{k}_c}\,\frac{1}{\Delta\phi_{c,r}}\int_c^{\bar{r}} d\bar{r}'\,\frac{d\phi}{d\bar{r}'}\,\bar{r}'^{a}\right], \tag{28}$$

to be used in the expression

$$T/T_c = (n/n_c)^{\Gamma-1} = 1 + (\Gamma-1)\,\beta_c\,\Delta\phi_{c,r}/\Gamma. \tag{29}$$

In the outer regions, a similar expansion may be pursued both for CC and NCC clusters to yield an effective index

$$\Gamma \simeq 1 + \frac{2}{5}\,\frac{1}{\Delta\phi_{r,R}}\int_{\bar{r}}^{1} d\bar{r}'\,\frac{d\phi}{d\bar{r}'}\,\bar{r}'^{-3a/5}. \tag{30}$$

In fact, Figure 3 last panel shows that values roughly constant in the range $\Gamma = 1.1$–1.2 apply to the outer regions of all cluster categories.[5]

Another approximation of the polytropic type is seen to apply for $r > r_m$, i.e., to the right of the peak of σ^2 (see Figure 1), and may be formally based as follows. Consider that wherever density and temperature follow (piecewise) power-law runs, the elimination of r provides a link of the polytropic form $n\,T \propto n^{\Gamma}$; a similar consideration applies to the DM, leading to define a corresponding index Λ. Thus, we may write the first and the third sides of Equation (2) in these terms, and equate them *directly*; then simple algebra provides the explicit relation

$$\frac{T}{T_m} \approx \beta_m\,\frac{\Lambda}{\Gamma}\,\frac{\Gamma-1}{\Lambda-1}\left(\frac{\sigma}{\sigma_m}\right)^2 + \frac{T_R}{T_m}. \tag{31}$$

This, complementarily to Equation (24), shows that the temperature run $T(r)$ tends to follow the DM dispersion $\sigma^2(r)$ except for the vicinity of the virial boundary where the shock condition sustains it at the value T_R, and for the very center where a finite if small k_c matters.

Summarizing the trend highlighted by the limiting models, the passive *mirror* behavior of the ICP with $T \propto \sigma^2$ prevails unless is offset by energy inputs, as in fact occurs at the boundary for all clusters, and in the central region for the NCC clusters.

7. DISCUSSION AND CONCLUSIONS

This paper introduces a novel look to the astrophysics of galaxy clusters, in terms of both the α-profiles for the initially cold DM and of the Supermodel for the hot ICP.

As for the DM halos, we have taken up from LC09 the *physical* α-profiles. These are based on the Jeans equilibrium between self-gravity and pressure modulated by the DM "entropy" run $K(r) \propto r^{\alpha}$. The latter is found from many recent N-body simulations (recalled in Section 1) to apply with α closely constant within the halo body; we have semianalytically computed the halo two-stage development and obtained the narrow range $\alpha \approx 1.27$–1.3 from poor to rich clusters (see Section 2 for details). The ensuing α-profiles, depending on the key parameters α and c, provide density runs $\rho(r)$ that satisfy *physical* central and outer boundary conditions at variance with the empirical NFW formula, and also yield better fits to detailed data from

[5] For a quick evaluation of the index, consider that $\Gamma \equiv 5/3 + d\log k/d\log n = 5/3 - a_R/g_R = b_R/g_R$.

gravitational lensing in and around massive clusters (see Lapi & Cavaliere 2009b).

The ICP, on the other hand, settles to equilibrium within the gravitational wells associated with the α-profiles, under control from the thermodynamic entropy produced by boundary and central shocks driven by AGNs or major mergers, plus a possible preheating basal level (see Section 3). These *physical* effects may be compounded in the two-parameter form $\bar{k}(r) = \bar{k}_c + (1 - \bar{k}_c)\,\bar{r}^a$ with a ranging from 0.8 to 1.1. The resulting equilibrium may be concisely rendered as a trend for the ICP to follow the DM in the *passive* behavior $T(r) \propto \sigma^2(r)$, in the radial range *free* from the energy inputs that steadily produce the *outer* boundary slope and intermittently refresh the *central* level $\bar{k}_c$.

In detail, our Supermodel of Section 4 provides accurate and extended representations for the runs of ICP temperature and density and of the related ICP observables (see Figure 5–7, for example). These validate the assumption of hydrostatic equilibrium, and closely constrain, in addition to the value of the concentration c for the DM α-profile, also the *two* ICP parameters a and $\bar{k}_c$. In fact, such representations hold for either NCC and CC clusters, marked out, respectively, by a *monotonic* outer decline of $T(r)$ from a central plateau at $T_c \gtrsim T_R$, or by a middle *peak*. In the Supermodel, these morphologies are produced by the central entropy k_c being higher or lower than a threshold value $k_c \approx$ 20–50 keV cm^2; correspondingly, the X-ray brightness features a flat core-like or a steep central run, based upon the *same* mildly cusped DM α-profile. In a forthcoming paper, we will present a detailed analysis of an extended sample of clusters, specifically NCC and UNC, with the aims of disentangling the origin of the central energy inputs, and of evaluating the variance in the cluster ages through their outer DM concentrations (see Section 2).

We stress that the Supermodel *inversely* links the runs of $T(r)$ and $n(r)$ toward the central region (see Section 4); in particular, it yields for the very central values the scaling $T_c \propto k_c^{0.35}$ and $n_c \propto k_c^{-1}$, implying $t_c \propto k_c^{1.2}$ for the cooling time. The stability of such values is argued in Section 5. High T_c combines with flat n_c to produce in NCC clusters central conditions conducive to *saturation* of k_c toward values around 10^2 keV cm^2. In CC clusters, instead, low though *finite* T_c combines with high n_c into a condition paving the way to fast cooling; this condition is conducive to triggering intermittent, recurrent loops going through the stages: cooling, massive BH fueling, AGN energy feedback, which halts further fueling and activity; these loops make possible in the long term a quasi-steady state. In the center of NCC clusters, instead, hot conditions suppress AGN reactivations owing to lack of dense cool ICP crowded around the central cluster galaxies; in addition, they tend to saturate the effective energy coupling from the most powerful AGNs or mergers by preventing or impairing supersonic conditions conducive to strong shocks.

Concerning central conditions, we emphasize two points. First, in CC clusters the Supermodel predicts a *finite* (nonzero) central T_c with no need for any twist in cooling flow theories, but rather constitutes a natural condition set by their equilibria at low k_c and stabilized against cooling by recurrent AGN activity. Second, in NCC clusters we expect *saturation* to enforce stability of the higher k_c levels set by the inputs from powerful AGNs and from the stronger if rarer substantial mergers.

Moving into the middle radial range where energy sources may be neglected, the "mirror" behavior of Equations (24) and (31) prevails with $T(r)$ *passively* following $\sigma^2(r)$; a novel feature emerging from the Supermodel is the very close location of the two respective peaks. This is because such two homologous quantities arise from a *parallel* response to the requirement of withstanding the common gravity for equilibrium (see Section 6, also Figure 3). This gravity-induced behavior is at the root of the remarkable effectiveness of the simple model $T(r) \propto \sigma^2(r)$, which for the CC clusters holds toward the center (see Figure 6). As a consequence, the Supermodel predicts the peak of $T(r)$ to move toward progressively *smaller* radii in going from rich clusters to groups.

On approaching the boundary, the run of $T(r)$ again deviates upward from this passive trend (see Section 3.1 and Appendix B), with a boundary value T_R sustained by the energy input associated to infall. Here, the passive ICP behavior is again expected to be broken by the energy transfer due to electromagnetic interactions and *localized* to a range $\Delta r \sim \lambda_{\rm pp} \ll r$ (whilst bubbles or shocks starting from the center smear their energy out to some 10^2 kpc, implying an effective $\Delta r/r \sim 1$). However, pinning down the outer deviations requires high sensitivity, currently achievable only with full use of the *Suzaku* capabilities.

Next, we highlight an unexpected *connection* specifically emerging from the Supermodel. X-ray observations of clusters yield information concerning the concentration c through the values of the outer entropy slope a, and more directly from detailed fits to the surface brightness data; in fact, we expect a to be *lower* and the density profile to be steeper for early clusters with *higher* concentrations c (see Section 3, in particular below Equations (13)). This specific prediction may be tested through extended simulations covering high-c halos and nonadiabatic processes as discussed, e.g., by Borgani (2007). In parallel, high concentrations are keenly pinpointed by gravitational lensing observations (Lapi & Cavaliere 2009b and references therein). This opens the way to the use of existing X-ray data as convenient pointers to targets for time-expensive gravitational lensing observations.

To conclude, we turn to contrasting the ICP and the DM behaviors. Note that the two density runs $\rho(r) \propto [\sigma^2(r)/K(r)]^{3/2}$ and $n(r) \propto [k_{\rm B}T(r)/k(r)]^{3/2}$ will *differ* even where $T \propto \sigma^2$ applies, to the extent that the DM and ICP entropy runs differ. This brings us to directly compare these two governing entropies.

In a nutshell, their *common* features stem from smooth, slow gravitational mass infall onto the outskirts, while their detailed runs both in the outer and in the central range reflect their different sensitivity to other energy inputs. Quantitatively, both the underlying key parameters b_R and $\kappa_{\rm crit}$ are amenable to *conversion* of infall kinetic energy. They take on very close values $b_R \approx$ 2.65–2.55 (see Section 3) and $\kappa_{\rm crit} \approx$ 2.6–2.5 (see Section 2) at their corresponding fiducial points $r \approx R$ or $r = r_p$; for increasing α or concentration c, they decrease together since both depend on $1/\Delta\phi$ in terms of the relevant potential drops from the turning point to R or r_p (see Equation (10) for the ICP and Equation (13) in LC09 for the DM).

On the other hand, the *differing* features stem from local versus nonlocal character of the energy conversion. The collisionless DM particles fall from the cluster surroundings well into the body, where their kinetic energy is *nonlocally* and progressively randomized, and spreads out entropy by orbit superposition and stratification with widely distributed apocenters (see LC09 and references therein). Correspondingly, in the DM halos $K(r) \equiv \sigma^2/\rho^{2/3}$ starts out in the outskirts with uniform values $\alpha \sim 1.1$ in all clusters, to *steepen*

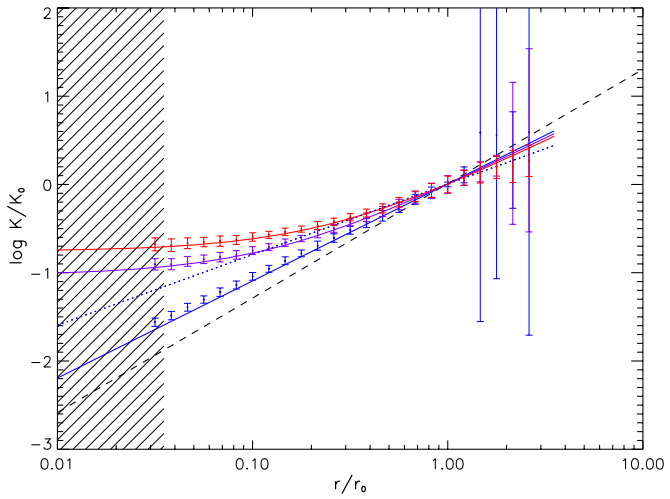

Figure 8. Reconstruction of the entropy profiles from joint X-ray and SZ observations (Cavaliere et al. 2005, see their Equation (8)). The dashed line shows the DM entropy profile with the slope $\alpha = 1.3$. The solid lines are the input ICP entropy profiles described by Equation (17), for our standard values $\bar{k}_c = 5 \times 10^{-2}$ (red), $\bar{k}_c = 2.5 \times 10^{-2}$ (cyan), and $\bar{k}_c = 0$ (blue); the error bars illustrate the reliability of the reconstruction from joint mock observations in a rich cluster at 1 Gpc of the X-ray brightness with resolution of $1''$ and sensitivities $\Delta I_X = 2 \times 10^{-4}\, I_{Xc}$, and of the SZ effect with resolution of $10''$ and sensitivities $\Delta I_y = 10^{-2}\, I_{yc}$. The blue dotted line represents an alternative ICP entropy profile with $a = 0.8$ (and $\bar{k}_c = 0$) as we expect for ICP preheated at 1/2 keV per particle (see Section 3.1.1); similar shapes have been observed by Sun et al. (2009) in many poor clusters, and by Lemze et al. (2008) in A1689.

(A color version of this figure is available in the online journal.)

toward the body to universal values 1.27–1.3 in a gently convex shape.[6]

Meanwhile, in the ICP $k(r) \equiv k_B T/n^{2/3}$ starts out at the boundary $r \approx R$ from somewhat lower average values $a \approx 1.1$–1.2, but with a considerable *variance* when large preheating and high DM concentrations are included, see Section 3.1.1 and evidence referred to therein. The slope, if anything, *flattens* out toward an effective value $a \approx 0$ in the presence of central energy inputs.

Beyond details, this concave versus convex shape of a toward the center, together with the sensitivity of its boundary values to outer potential and preheating constitute features specific to the ICP. Thus, we conclude that basically *similar* gravitational processes in DM and ICP (randomization of bulk kinetic energy, but on different scales) with the addition of the ICP collisional sensitivity to other energy inputs, concur to produce *dissimilar* shapes for $K(r)$ and $k(r)$.

Model independently, we propose two observational tests addressed at *directly* probing in clusters the two underlying entropies. The run $K(r)$ of the DM entropy can be derived from probing the α-profile by gravitational lensing observations as recalled in Section 2. The run $k(r)$ of the ICP entropy can be reconstructed as proposed by Cavaliere et al. (2005) and illustrated in Figure 8 starting from the relation

$$k(r) = \mathcal{Y}^{14/9}(r)\, \mathcal{L}_X^{-10/9}(r), \tag{32}$$

which joins deconvolved observations of X-ray brightness and SZ effect irrespective of any modeling or assumption on hydrostatic equilibrium and of redshift information. Such studies may be particularly useful in the ongoing search for early clusters (see Andreon et al. 2009).

[6] Note that our slope of $K \equiv \sigma^2/\rho^{2/3}$ defined in terms of the one-dimensional velocity dispersion is consistent with that in terms of the three-dimensional dispersion, e.g., Faltenbacher et al. (2007); in detail, Dehnen & McLaughlin (2005) and Ascasibar & Gottlöber (2008) find the latter to be somewhat flatter than the former in the outer body where radial anisotropies tend to prevail.

Table 1
Fit Parameters of Equation (A1)

	$c = 3.5$			$c = 4.5$			$c = 5.5$		
$\bar{k}_c$	A_0	A_1	A_2	A_0	A_1	A_2	A_0	A_1	A_2
0	17.77	2.86	0.49	22.82	2.72	0.47	27.59	2.64	0.47
10^{-4}	17.47	2.86	0.49	22.33	2.71	0.48	26.88	2.63	0.48
10^{-3}	15.93	2.83	0.54	19.99	2.66	0.54	23.72	2.56	0.53
5×10^{-3}	13.42	2.73	0.62	16.53	2.51	0.61	19.34	2.38	0.61
10^{-2}	12.04	2.63	0.66	14.70	2.39	0.66	17.09	2.25	0.65
2.5×10^{-2}	10.06	2.44	0.72	12.14	2.18	0.71	13.99	2.02	0.71
5×10^{-2}	8.53	2.26	0.77	10.19	1.99	0.75	11.66	1.83	0.74
7.5×10^{-2}	7.64	2.14	0.79	9.08	1.87	0.77	10.34	1.71	0.76
10^{-1}	7.03	2.05	0.81	8.31	1.78	0.79	9.44	1.62	0.77

Notes. In computing the integral in Equation (8), we have used the DM α-profiles with $\alpha = 1.27$. The above fitting coefficients are given for three values of the concentration parameter; other values may be derived by standard interpolation techniques.

We thank an anonymous referee for keen comments and helpful suggestions. We have benefitted from various exchanges with A. Biviano, S. Borgani, A. Diaferio, M. Norman, Y. Rephaeli, and P. Rosati. Work partially supported by Agenzia Spaziale Italiana (ASI) and Istituto Nazionale di Astrofisica (INAF). A.L. thanks INAF-OATS for kind hospitality.

APPENDIX A

THE INTEGRAL IN EQUATION (8)

Here, we provide an effective approximation to the integral $I(r)$ appearing on the right-hand side (rhs) of Equation (8), in terms of the following analytical expression

$$I(\bar{r}) \equiv \int_{\bar{r}}^{1} \frac{d\bar{r}'}{\bar{r}'} \bar{v}_c^2(\bar{r}') \bar{k}^{-3/5}(\bar{r}') \simeq A_0 \exp\left(-A_1 \bar{r}^{A_2}\right) \tag{A1}$$

the fitting parameters A_0, A_1, and A_2 depend weakly on $\bar{k}_c$, as specified in Table 1. The dotted lines in Figure 2 (top panel) illustrate the effectiveness of such an approximation for our three standard values of $\bar{k}_c$. Note that on approaching the center the integral is numerically found to scale with central entropy k_c like $I_c \propto k_c^{-1/4}$, see Figure 2 (bottom panel). This result is used in Section 4 of the main text.

We plan to provide elsewhere a set of fitting formulae for $\rho(r)$ and $v_c^2(r)$ leading to an analytic expression for $I(r)$, as tools enabling direct data analysis and extensive precision fits.

APPENDIX B

ENTROPY PRODUCTION IN SHOCKS

While cooling may condense the colder fractions of the ICP and indirectly raise the average entropy of the rest, it is generally agreed (see Cavaliere et al. 2002; Voit 2005) that substantial entropy production requires shock waves. Here, we recall from LCM05 the temperature, density, and entropy jumps produced across a shock transitional layer.

Conservation of mass, energy, and total stress across the latter lead to the classic Rankine–Hugoniot temperature jump

$$\frac{T_2}{T_1} = \frac{5}{16}\,\tilde{\mathcal{M}}^2 + \frac{7}{8} - \frac{3}{16}\,\frac{1}{\tilde{\mathcal{M}}^2}. \tag{B1}$$

The subscripts 1 and 2 denote the pre- and postshock quantities, and $\tilde{\mathcal{M}} \equiv (3\,\mu m_p\,\tilde{v}_1^2/5\,k_{\rm B}T_1)^{1/2}$ the shock Mach number; the quantities with tildes refer to the *shock* reference frame, which is convenient in the case of internal shocks driven, e.g., by AGNs.

On the other hand, in the case of accretion shocks it is more convenient to work in terms of the infall velocity v_1 and of the related Mach number $\mathcal{M} \equiv (3\,\mu m_p\,v_1^2/5\,k_{\rm B}T_1)^{1/2}$ measured in the *center of mass* frame. Assuming the downstream kinetic energy to be small, one finds the temperature jump in the form

$$\frac{T_2}{T_1} = 1 + \frac{4}{9}\,\mathcal{M}^2\left[\frac{1}{4} + \sqrt{1 + \frac{9}{4}\,\frac{1}{\mathcal{M}^2}}\right]. \tag{B2}$$

In either reference frame the density jump in terms of the pre- and postshock temperatures reads

$$\frac{n_2}{n_1} = 2\left(1 - \frac{T_1}{T_2}\right) + \sqrt{4\left(1 - \frac{T_1}{T_2}\right)^2 + \frac{T_1}{T_2}}. \tag{B3}$$

The entropy jump $K_2/K_1 = (T_2/T_1)/(n_2/n_1)^{2/3}$ may be easily composed from the relations above.

Handy expressions apply to *strong* shocks, when the above expressions reduce to

$$\frac{T_2}{T_1} \simeq \frac{3}{16}\,\frac{\mu m_p\,\tilde{v}_1^2}{k_{\rm B}T_1} + \frac{7}{8} \simeq \frac{1}{3}\,\frac{\mu m_p\,v_1^2}{k_{\rm B}T_1} + \frac{3}{2},\quad \frac{n_2}{n_1} \simeq 4\left(1 - \frac{15}{16}\,\frac{T_1}{T_2}\right); \tag{B4}$$

these approximations actually apply to high/intermediate $\tilde{\mathcal{M}}^2 \gtrsim 3$; the corresponding entropy jumps read

$$\frac{K_2}{K_1} \simeq \frac{3}{16}\,\frac{1}{4^{2/3}}\,\frac{\mu m_p\,\tilde{v}_1^2}{k_{\rm B}T_1} + \frac{3}{2}\,\frac{1}{4^{2/3}} \simeq \frac{1}{3}\,\frac{1}{4^{2/3}}\,\frac{\mu m_p\,v_1^2}{k_{\rm B}T_1} + \frac{17}{8}\,\frac{1}{4^{2/3}}. \tag{B5}$$

In last relation, the second term on the rhs expresses the contributions of the advected external entropy $0.84K_1$, and is relevant when $k_{\rm B}T_1 \gtrsim 0.16\,m_p v_1^2$, that is, when relatively strong preheating affects the gas infalling into a poor cluster or a group.

When a central energy pulse is discharged into the equilibrium ICP with a density gradient, e.g., $n(r) \propto r^{-2}$, a blast wave is sent out; that is, a nonlinear perturbed flow that terminates into a leading shock and comprises bulk kinetic energy up to matching the thermal one (see Sedov 1959). When the pulse is short compared with the transit time and the effects of gravity and upstream pressure are neglected, the Mach number decreases radially as $\mathcal{M}(r) \propto r^{-1/2}$. When the pulse is sustained during the transit time, $\mathcal{M}(r)$ will also be. Even with gravity and upstream pressure considered, this is found to hold in the simple case of a pulse constant over the transit time through the region where $n(r) \propto r^{-2}$ applies, and to hold also for other combinations of equilibrium gradients and pulse shapes (LCM05). For longer times, $\mathcal{M}(r)$ declines and the blast dissipates its kinetic energy into the ICP.

In such cases, the Mach number depends on the energy input ΔE relative to the ICP total energy E in the affected volume, simply as $\mathcal{M}^2 \approx 1 + \Delta E/E$; the condition for a strong shock $\mathcal{M}^2 \gtrsim 3$ clearly translates into $\Delta E/2\,m\,k_{\rm B}T \gtrsim 1$. It turns out that the ICP may be (partly) evacuated from the central region to a residual average density $n(1 - \Delta n/n) \propto 1 - \Delta E/2\,E$, with an associated entropy $k_c \propto \Delta E/(1 - \Delta E/2\,E)^{2/3}$.

REFERENCES

Andreon, S., Maughan, B., Trinchieri, G., & Kurk, J. 2009, MNRAS, submitted (arXiv:0812.1699)
Ascasibar, Y., & Gottlöber, S. 2008, MNRAS, 386, 2022
Babul, A., et al. 2002, MNRAS, 330, 329
Balogh, M. L., Babul, A., & Patton, D. R. 1999, MNRAS, 307, 463
Balogh, M., Mc Carthy, I. G., Bower, R., & Voit, G. M. 2007, in Heating Versus Cooling in Galaxies and Clusters of Galaxies, ESO Astrophysics Symposia ed. H. Böhringer et al. (Berlin: Springer), 268
Binney, J. 1978, MNRAS, 183, 779
Binney, J., & Tabor, G. 1995, MNRAS, 276, 663
Blanchard, A., Valls-Gabaud, D., & Mamon, G. A. 1992, A&A, 264, 365
Borgani, S. 2007, in Heating Versus Cooling in Galaxies and Clusters of Galaxies, ESO Astrophysics Symposia, ed. H. Böhringer et al. (Berlin: Springer), 339
Broadhurst, T., et al. 2008, ApJ, 685, L9
Bryan, G. L. 2000, ApJ, 544, L1
Cavagnolo, K. W., Donahue, M., Voit, G. M., & Sun, M. 2009, ApJS, 182, 12
Cavaliere, A., & Fusco-Femiano, R. 1976, A&A, 49, 137
Cavaliere, A., & Fusco-Femiano, R. 1978, A&A, 70, 677
Cavaliere, A., & Fusco-Femiano, R. 1981, A&A, 100, 194
Cavaliere, A., Gursky, H., & Tucker, W. 1971, Nature, 231, 437
Cavaliere, A., Lapi, A., & Rephaeli 2005, ApJ, 634, 784
Cavaliere, A., & Lapi, A. 2008, ApJ, 673, L5
Cavaliere, A., Lapi, A., & Menci, N. 2002, ApJ, 581, L1
Cavaliere, A., Menci, N., & Tozzi, P. 1999, MNRAS, 308, 599
Ciotti, L., & Ostriker, J. P. 2001, ApJ, 551, 131
Ciotti, L., & Ostriker, J. P. 2007, ApJ, 665, 1038
Conroy, C., & Ostriker, J. P. 2008, ApJ, 681, 151
Dehnen, W., & McLaughlin, D. E. 2005, MNRAS, 363, 1057
Diemand, J., Kuhlen, M., & Madau, P. 2007, ApJ, 667, 859
Dos Santos, S., & Doré, O. 2002, A&A, 383, 450
Dwight, H. B. 1961, Mathematical Tables of Elementary and Some Higher Mathematical Functions (New York: Dover)
Ettori, S., & Fabian, A. C. 1998, MNRAS, 293, L33
Faltenbacher, A., Hoffman, Y., Gottloeber, S., & Yepes, G. 2007, MNRAS, 376, 1327
Forman, W., et al. 2005, ApJ, 635, 894
Gastaldello, F., Buote, D. A., Brighenti, F., & Mathews, W. G. 2008, ApJ, 673, L17
Giacintucci, S., et al. 2008, ApJ, 682, 186
Gursky, H., et al. 1972, ApJ, 173, L99
Hansen, S. H., & Moore, B. 2006, New Astron., 11, 333
Hansen, S. H., & Piffaretti, R. 2007, A&A, 476, L37
Hoffman, Y., Romano-Díaz, E., Shlosman, I., & Heller, C. 2007, ApJ, 671, 1108
Høst, O., et al. 2009, ApJ, 690, 358
Lapi, A., & Cavaliere, A. 2009a, ApJ, 692, 174 (LC09)
Lapi, A., & Cavaliere, A. 2009b, ApJ, 695, L125
Lapi, A., Cavaliere, A., & Menci, N. 2005, ApJ, 619, 60 (LCM05)
Leccardi, A., & Molendi, S. 2008, A&A, 486, 359
Lemze, D., Barkana, R., Broadhurst, T. J., & Rephaeli, Y. 2008, MNRAS, 386, 1092
Markevitch, M., & Vikhlinin, A. 2007, Phys. Rep., 443, 1
McCarthy, I. G., et al. 2004, ApJ, 613, 811
McCarthy, I. G., et al. 2007, MNRAS, 376, 497
McCarthy, I. G., et al. 2008, MNRAS, 386, 1309
McNamara, B. R., & Nulsen, P. E. J. 2007, ARA&A, 45, 117
Mitchell, R. J., Culhane, J. L., Davison, P. J. N., & Ives, J. C. 1976, MNRAS, 175, 29
Mittal, R., Hudson, D. S., Reiprich, T. H., & Clark, T. 2009, A&A, in press (arXiv:0810.0797)
Molendi, S., & Pizzolato, F. 2001, ApJ, 560, 194
Nagai, D., Kravtsov, A. V., & Vikhlinin, A. 2007, ApJ, 668, 1
Navarro, J. F., Frenk, C. S., & White, S. D. M. 1997, ApJ, 490, 493
Navarro, J. F., et al. 2009, MNRAS submitted (arXiv:0810.1522)
Nulsen, P. E. J., et al. 2005, ApJ, 625, L9
Nusser, A., Silk, J., & Babul, A. 2006, MNRAS, 373, 739
Ostriker, P. O., Bode, P., & Babul, A. 2005, ApJ, 634, 964
Peterson, J. R., & Fabian, A. C. 2006, Phys. Rep., 427, 1
Ponman, T. J., Sanderson, A. J. R., & Finoguenov, A. 2003, MNRAS, 343, 331

Pratt, G. W., & Arnaud, M. 2003, A&A, 408, 1
Pratt, G. W., Croston, J. H., Arnaud, M., & Boehringer, H. 2009, A&A, in press (arXiv:0809.3784)
Rasmussen, J., & Ponman, T. J. 2004, MNRAS, 349, 722
Richards, G. T., et al. 2006, AJ, 131, 2766
Sarazin, C. L. 1988, X-ray Emission from Clusters of Galaxies (Cambridge: Cambridge Univ. Press)
Scannapieco, E., & Oh, S. P. 2004, ApJ, 608, 62
Sedov, L. I. 1959, Similarity and Dimensional Methods in Mechanics (New York: Academic)
Serlemitsos, P. J., et al. 1977, ApJ, 211, L63
Spergel, D. N., et al. 2007, ApJS, 170, 377
Sun, M., et al. 2009, ApJ, 693, 1142
Sunyaev, R. A., & Zel'dovich, Y. B. 1972, Comments Astrophys. Space Phys., 4, 173
Taylor, J. E., & Navarro, J. F. 2001, ApJ, 563, 483
Tormen, G., Moscardini, L., & Yoshida, N. 2004, MNRAS, 350, 1397
Tozzi, P., & Norman, C. 2001, ApJ, 546, 63
Tucker, W., Tananbaum, H., & Fabian, A. 2007, Sci. Am., 296, 42
Valageas, P., & Silk, J. 1999, A&A, 350, 725
Vass, I. M., Valluri, M., Kravtsov, A. V., & Kazantzidis, S. 2009, MNRAS, in press (arXiv:0810.0277)
Voit, G. M. 2005, Rev. Mod. Phys., 77, 207
Voit, G. M. 2008, in The Warm and Hot Universe (New York: Columbia Univ.), http://warmhot.gsfc.nasa.gov
Voit, G. M., & Bryan, G. L. 2001, Nature, 414, 425
Voit, G. M., & Donahue, M. 2005, ApJ, 634, 955
Voit, G. M., et al. 2002, ApJ, 576, 601
Voit, G. M., et al. 2003, ApJ, 593, 272
White, S. D. M., & Rees, M. J. 1978, MNRAS, 183, 341
Wu, K. K. S., Fabian, A. C., & Nulsen, P. E. J. 2000, MNRAS, 318, 889
Zhang, Y.-Y., et al. 2008, A&A, 482, 451
Zhao, D. H., Mo, H. J., Jing, Y. P., & Börner, G. 2003, MNRAS, 339, 12